Nanoscale

COMMUNICATION

View Article Online
View Journal | View Issue

Check for updates

Cite this: *Nanoscale*, 2018, **10**, 2260

Received 3rd December 2017, Accepted 27th December 2017

DOI: 10.1039/c7nr08997j

rsc.li/nanoscale

Direct observation of the topological spin configurations mediated by the substitution of rare-earth element Y in MnNiGa alloy

S. L. Zuo,[a,b] Y. Zhang, *[a] L. C. Peng, [a,b] X. Zhao,[a,b] R. Li,[a,b] H. Li,[a,b] J. F. Xiong,[a,b] M. He,[a,b] T. Y. Zhao,[a] J. R. Sun, [a,b] F. X. Hu[a,b] and B. G. Shen*[a,b]

The evolution of topological magnetic domains microscopically correlates the dynamic behavior of memory units in spintronic application. Nanometric bubbles with variation of spin configurations have been directly observed in a centrosymmetric hexagonal magnet $(Mn_{0.5}Ni_{0.5})_{65}(Ga_{1-y}Y_y)_{35}$ (y = 0.01) using Lorentz transmission electron microscopy. Magnetic bubbles instead of biskyrmions are generated due to the enhancement of quality factor Q caused by the substitution of rare-earth element Y. Furthermore, the bubble density and diversified spin configurations are systematically manipulated *via* combining the electric current with perpendicular magnetic fields. The magnetic bubble lattice at zero field is achieved after the optimized manipulation.

1. Introduction

Recently, nanoscale topological magnetic spin configurations such as vortices, bubbles and skyrmions have received intensive attention from the viewpoint of both fundamental science and potential applications in the magnetic recording and memory devices.[1] The spin angular momentum of the charge carriers (such as electrons) can be transferred to a magnetic structure to drive and manipulate the topological configuration (such as magnetic skyrmion) *via* the spin transfer torque or spin Hall torque effects,[2,3] thus showing their significant application as racetrack memory devices.[4] The threshold current density to drive the skyrmion motion can be as low as $(10^5–10^6\ \mathrm{A\ m^{-2}})$,[5–7] saving much energy compared with traditional domain wall movement $(10^{10}–10^{11}\ \mathrm{A\ m^{-2}})$.

The conventional magnetic bubbles studied as memory units for data storage in the 1970s[8–10] are usually of micro size with the dominating up and down magnetization separated by a negligible width of the domain wall in a cylinder, which is closely related to magnetic dipolar interactions. The spontaneous magnetization M_S, uniaxial anisotropy K_u, exchange stiffness A, and sample thickness h are usually specified for magnetic bubbles in terms of the following requirements,[11] as indicated by the domain theory and experimental observation: (i) the easy axis of magnetic anisotropy being spontaneously perpendicular to the film plane, with the so-called quality factor $Q = K_u/K_d \geq 1$, where K_d is the stray field energy given by $\mu_0 M_S^2/2$, where μ_0 is the vacuum permeability; (ii) an appropriate thickness $h \sim 4l_c$, where l_c is the characteristic length parameter of the material given by $l_c = \gamma_w/(2K_d)$, where $\gamma_w = 4(AK_u)^{1/2}$ is the specific domain wall energy; and (iii) a relatively lower coercive force in the viewpoint of magnetic domain wall dynamics. Additionally, magnetic bubbles also exist in some materials with the Q slightly lower than 1, such as thin cobalt crystals and hexaferrites.[8,10,12,13]

With the recent progress in magnetic skyrmions, the magnetic bubbles with nanoscale sizes and their topological properties are further studied.[4,5,7,14–16] The theoretical simulation[14,17] and experimental results[5,7,15] have demonstrated that nontrivial magnetic bubbles can be topologically equivalent to magnetic skyrmions, possessing similar integral topological numbers and electrically driven behaviour. Magnetic stripe or labyrinth domains are the ground state and evolve into skyrmions or bubbles by applying an external magnetic field if the intrinsic magnetic interaction is appropriate.[7]

The in-plane magnetization of the three-dimensional skyrmion configuration is in the form of a vortex-like texture with an integral topological number. Skyrmions have been predominantly studied in chiral-lattice magnets such as MnSi,[18–21] FeGe,[22,23] FeCoSi,[24] where the Dzyaloshinsky–Moriya interactions (DMI) originate from the noncentrosymmetric crystal structure. Skyrmions have also been explored in centrosymmetric materials with uniaxial magnetic anisotropy and dipolar interactions.[5,7,25–29] Room temperature skyrmions can be easily obtained in the interfacial-DMI determined multilayers.[30] Skyrmions stabilized at zero field were studied *via* external-field manipulations or within confined patterns due to the edge constriction.[28,31,32] For the diversified applications of topological skyrmions, it is highly desirable to expand

[a]*State Key Laboratory for Magnetism, Institute of Physics, Chinese Academy of Sciences, Beijing 100190, P. R. China. E-mail: shenbg@iphy.ac.cn, zhangy@iphy.ac.cn*
[b]*University of Chinese Academy of Sciences, Beijing, 100049, P. R. China*

the horizon of new materials and possible topology manipulations.

The quality factor $Q = K_u/K_d = 2K_U/\mu_0 M_S^2$ is proposed as a crucial parameter to stabilize a certain topological spin configuration.[14] Magnetization direction and rotation can be tailored *via* magnetic anisotropy, leading to different spin configurations.[5,7,14] A number of theoretical simulations and experimental manipulations[33–35] suggest that the skyrmion configuration could be controlled by external stimuli such as electric currents,[36] magnetic fields,[37] and thermal gradients, which microscopically correlates with the dynamic behaviour of the information unit in actual application.[38,39] Magnetic bubbles in place of biskyrmions were observed at low temperatures *via* field-cooling manipulation in tetragonal ($I4/mmm$) manganite $La_{2-2x}Sr_{1+2x}Mn_2O_7$ (x = 0.315),[4] implying a good arena to tune the skyrmion configuration and spin helicity in dipolar magnets.

Recently the biskyrmion configuration and manipulation in a super-wide temperature range have been systematically studied in a centrosymmetric $(Mn_{1-x}Ni_x)_{65}Ga_{35}$ (x = 0.5) (MnNiGa) alloy.[27,33,40] To take better advantage of these topological magnetization textures in spintronic devices, the present work explores the spin configuration manipulation in a rare-earth element Y substituted MnNiGaY alloy. The spin configuration transition from biskyrmions in MnNiGa to bubbles in MnNiGaY is investigated, contributing to the enhancement of the quality factor Q. Moreover, the spin configuration manipulation behaviour of magnetic bubbles is extensively demonstrated by applying an electric current with the assistance of a magnetic field using Lorentz transmission electron microscopy (LTEM), generating a zero-field bubble lattice under optimized conditions.

2. Experimental

A polycrystalline hexagonal $(Mn_{0.5}Ni_{0.5})_{65}(Ga_{1-y}Y_y)_{35}$ (y = 0.01) (MnNiGaY) alloy was prepared by an arc melting technique under a high-purity argon atmosphere, which is the same as that used for the MnNiGa alloy.[27,33] The thin plate for the LTEM observation was cut from the polycrystalline ingot and thinned by mechanical polishing and argon ion milling. The magnetic domain studies are performed within a single grain of the foil sample since the grain size is much larger than that of the spot area in the TEM. Magnetic textures were investigated at room temperature using a LTEM (JEM 2100, JEOL) with an electric-current TEM holder. The high-resolution magnetization textures were obtained *via* the analysis of LTEM images (the under-focus and over-focus images) in terms of the transport-of-intensity equation (TIE). The objective lens was turned off when the sample holder was inserted and the perpendicular magnetic field was applied by gradually increasing the objective lens current. The magnetic properties of the polycrystalline ingots were measured by using a Quantum Design Physical Property Measurement System (PPMS, Quantum Design, Inc.) with a magnetic field up to 2 T. The spontaneous magnetization M_s was determined using $1/H$ plots. The singular point detection (SPD) technique[41–43] was employed to calculate the anisotropy of the oriented polycrystalline MnNiGaY samples, which are prepared by aligning the milled powders together with epoxy resin in a field of 1 T. The magnetization curves of the oriented samples were measured using a superconducting quantum interference magnetometer–vibrating sample magnetometer (SQUID-VSM).

3. Results and discussion

The spontaneous stripe domains at zero field and the complete biskyrmion state at a perpendicular magnetic field of 0.28 T are shown in Fig. 1a and b, respectively, consistent with the previous results for MnNiGa.[2] The spontaneous labyrinth domain structure (Fig. 1c) and varieties of magnetic bubble configurations (Fig. 1d) at a magnetic field of 0.39 T are observed in the rare earth Y substituted MnNiGaY. The same XRD spectrum and selected area diffraction patterns along the [001] zone-axis demonstrate that the crystal structure is not changed by Y substitution. Unfortunately, the accurate Y atom position has not yet been refined due to the very small amount of substitution. The TIE analysis of the labyrinth domain struc-

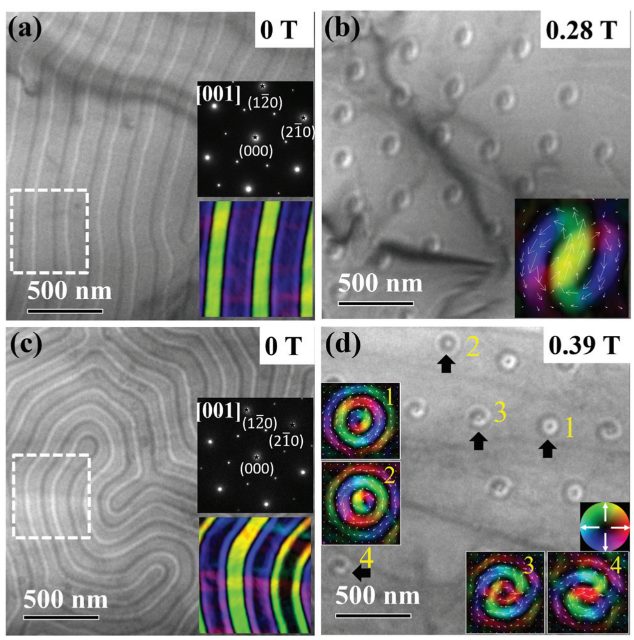

Fig. 1 Lorentz TEM images of magnetic domains in MnNiGa and MnNiGaY. The under-focused LTEM images of (a) spontaneous stripe domain structure and (b) complete biskyrmions at a magnetic field of 0.28 T in MnNiGa. (c) Spontaneous labyrinth domain structure at zero field and (d) bubbles at a magnetic field of 0.39 T in MnNiGaY. The selected area electron diffraction (SAED) (insets) indicating a [001] orientation. The in-plane magnetization of selected areas by TIE analysis (a) stripe, (b) biskyrmion, (c) labyrinth, and (d) numbered bubbles. The arrows and colors indicate the magnitudes and directions of the in-plane magnetizations, while the dark color indicates the magnetization along the perpendicular direction.

ture (the inset of Fig. 1c) reveals complex spin patterns, different from the periodic variation of the magnetization in the stripe domain in the inset of Fig. 1a. The large area of the dark contrast in the labyrinth domain structure indicates a large perpendicular magnetization region. The labyrinth domains pinch off resulting in the coexistence of labyrinth domains and magnetic bubbles while gradually increasing the magnetic field. At the magnetic field of 0.39 T, the magnetic labyrinth domains are completely replaced by bubble domains (Fig. 1d) with random distribution of different spin configurations (inset of Fig. 1d by the TIE method). The magnetization textures in bubbles "1" and "2" belong to type I bubbles and have three concentric rings with continuously opposite helicities, corresponding to the white or black contrast of the individual circles.[10] The three-dimensional spin texture for the type I bubble has been illustrated in ref. 5, counting the topological number (winding number) as one irrespective of the magnetic helicity.[6] Bubble "3" and bubble "4" have the opposite magnetization with a pair of Bloch lines between two halves of the domain wall, corresponding to type II bubbles with topological number zero.[10] The bubbles experimentally collapse into the ferromagnetic state above a critical magnetic field of 0.45 T. The theoretical collapsing magnetic field H_{co} for an ideal magnetic bubble can be approximately calculated using the Callen's expression[44] of stability, $\mu_0 H_{co} = \mu_0 M_S[1 + 3\lambda/4 - (3\lambda)^{1/2}]$, where λ is the dimensionless characteristic length given by $\lambda \equiv l_c/h$. With $h \sim 80$ nm and $l_c \sim 21.9$ nm, $\lambda \sim 0.274$ (see details in Notes†). The collapse field for magnetic bubbles in MnNiGaY is calculated to be about $0.299\mu_0 M_S$, *i.e.* 0.13 T, which is smaller than the LTEM result of ~0.45 T. The calculated collapse diameter[44] d_{co} is about 88.5 nm by using $d_{co} = 2h[(3/\lambda)^{1/2} - 3/2]^{-1}$, in good agreement with the experimentally observed bubble size. The relatively high collapse field observed in the experiments is probably because the in-plane Bloch line pairs in type II bubbles require a larger magnetic field to be oriented along the perpendicular direction, which is not considered in the Callen's expression.

The magnetization measurements are conducted to explore the origination of the spin configuration transition from biskyrmions to bubbles. The field dependence of the magnetization for the oriented polycrystalline magnets is shown in Fig. 2a, where the effective uniaxial anisotropy field H_k is determined by using the SPD technique as presented in the inset of Fig. 2a. The M_s is obtained by fitting the magnetization curves of fields higher than 1.0 T (Fig. 2b) according to the approach to the saturation law. By Y substitution, $\mu_0 M_s$ decreases from 0.547 to 0.434 T and $\mu_0 H_k$ increases from 0.38 to 0.43 T, which are consistent with the collapse magnetic fields for biskyrmions and bubbles. The calculated K_d drops from 119.1 to 74.8 kJ m^{-3} and the K_u decreases from 82.70 to 74.20 kJ m^{-3}. Therefore, the overall quality factor Q ($Q = K_u/K_d = \mu_0 H_k/\mu_0 M_S$) is found to be approximately 30% larger due to the substitution of rare earth element Y, from 0.69 for MnNiGa to 0.99 for MnNiGaY, which explains the origin of the spin configuration transition from biskyrmions to bubbles. However, in spite of the 30% enhancement of Q, the fact that the quality

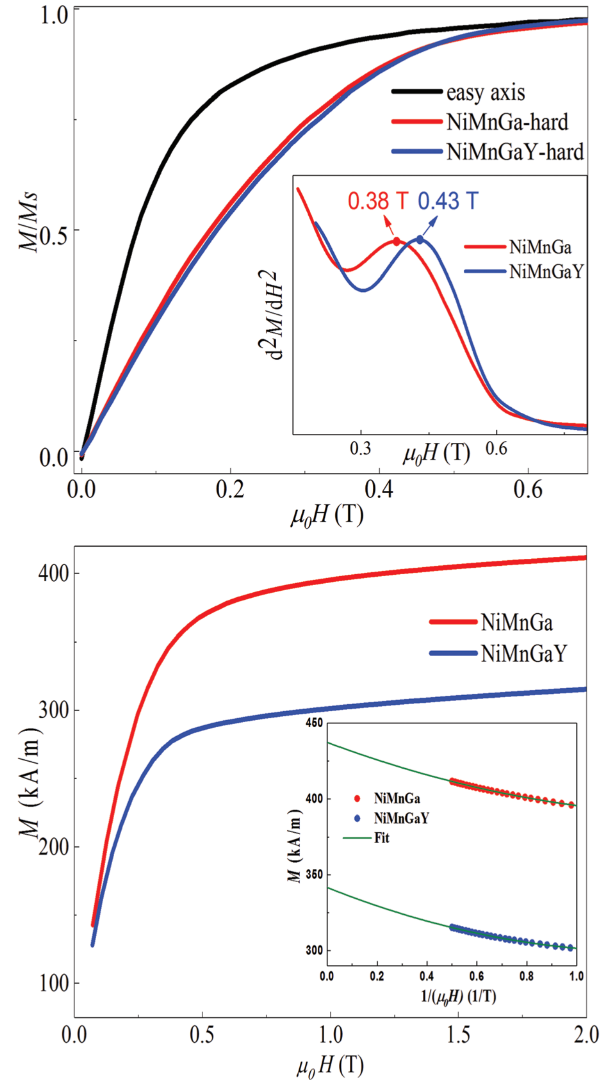

Fig. 2 Magnetic field dependence of the magnetization (M–H curve) at room temperature for (a) oriented samples measured parallel and perpendicular to the direction of easy magnetization, the inset demonstrating the second derivative (d^2M/dH^2) curves of perpendicular magnetization, and (b) isotropous bulk samples, the inset showing the M–$1/H$ curve.

factor Q of MnNiGaY is lower than 1.0 implies that MnNiGaY is different from previous conventional magnetic bubbles with strong perpendicular anisotropy materials and $Q \gg 1$.[13] These novel magnetic textures observed in MnNiGaY may encourage further exploration of new skyrmionic materials in accordance with the magnetic parameters.

Although various bubbles are observed at room temperature in the MnNiGaY alloy, their distribution is random. Therefore, external field manipulation is performed *via* a combination of in-plane electrical current and perpendicular magnetic field *via* LTEM. The residual state with mixed magnetic domains of labyrinths, dumbbells, and bubbles (Fig. 3a) is obtained after an appropriate manipulation. The residual state evolves into a complete bubble state (Fig. 3b) at the perpendicular magnetic

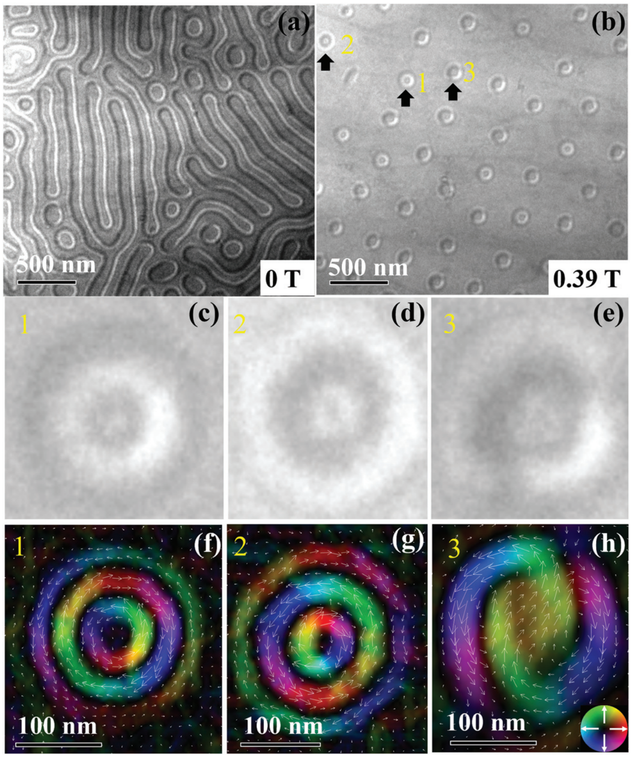

Fig. 3 Electromagnetic manipulation in MnNiGaY. LTEM images of (a) residual domains after the electric current manipulation and (b) the complete bubble state at a perpendicular magnetic field of 0.39 T based on the residual state. (c–e) Enlarged LTEM images of representative bubbles numbered in (b). (f–h) Corresponding magnetization textures obtained by TIE analysis. The magnitude and orientation of the magnetization are depicted by the colors and arrows referring to the color wheel in the inset.

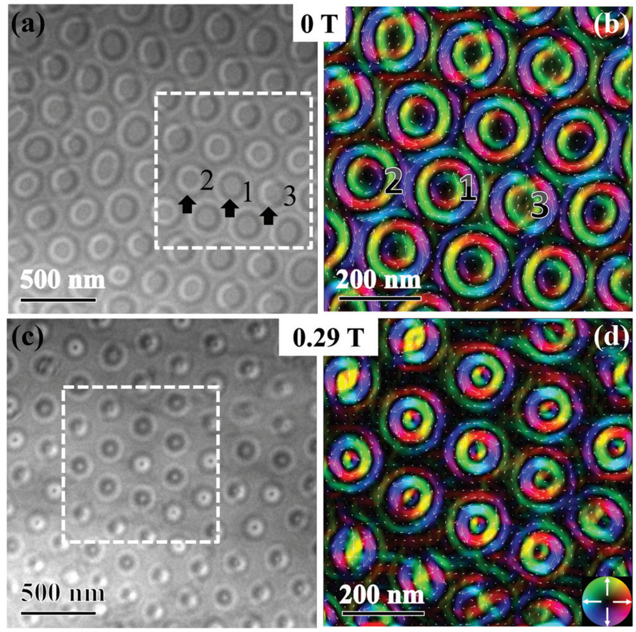

Fig. 4 High-density bubble lattice after an optimized electromagnetic manipulation with 50 mT constant magnetic field in MnNiGaY. (a) Under-focused LTEM images of the residual state and (b) the corresponding spin texture by TIE analysis of the box area. (c) Size-reduced bubble lattice and (d) corresponding spin texture of the box area after further increase of the magnetic field to 0.29 T.

field of 0.39 T. The bubble density becomes higher in comparison with that in Fig. 1d. The magnified in-plane magnetization textures *via* TIE analysis demonstrate similar type I bubbles (Fig. 3f and g) with clockwise and counterclockwise winding spins in three concentric rings. But the spin configuration of the type II bubble (Fig. 3h) with a pair of Bloch lines is a little different from that of bubbles "3" and "4" in the inset of Fig. 1d. The random distribution of the domain wall contrast originates from the equal opportunity for either helicity direction in the system.[5,7] The manipulation is conducted by increasing the electric current till the disappearance of the magnetic domains (150 mA, $J = 4.2 \times 10^7$ A m^{-2}) and then the current is switched off. Although the objective lens is off, the mixed magnetic domain state in Fig. 3a indicates a small remnant magnetic field, otherwise only labyrinth domains remain without any magnetic field.

The influence of the magnetic field on the manipulation is further investigated. A hexagonal bubble lattice is achieved under an optimized magnetic field of 50 mT (similar to Field cooling).[33] Moreover, the high density bubble lattice persists at zero field after switching off both the magnetic field and the electric current. The spin configurations are randomly distributed with type I and II magnetic bubbles shown in Fig. 4b. On further increasing the perpendicular magnetic field based on the zero-field residual state, the bubble size shrinks and vortex-like spin configurations concentrate at the core area (Fig. 4d). The bubble lattice collapses and then vanishes into a uniform ferromagnetic state above a critical magnetic field of 0.48 T. This intriguing behaviour of bubbles reorganizing themselves into a remarkably hexagonal lattice (Fig. 4) *via* electromagnetic manipulation provides an alternative option to generate patterned low-power consumption memory devices.

The stability and relaxation behaviours of the memory units should be considered in applications. The mixed magnetic bubble state containing dumbbells and type I and II bubbles with three configurations just after the above manipulation is shown in Fig. 5a. The bubble configuration changes with almost all type I bubbles transformed into type II (only one type I bubble left marked with a star) after 8-day relaxation as shown in Fig. 5c, which indicates that the type II bubble is stable in this material. Because of its singular nature, a type II bubble with a Bloch line has higher energy as in a Co thin film,[10] the peculiar generation of uniform type II bubble provides new insights to eliminate random configuration distribution.

A different electromagnetic manipulation procedure presents similar effects to obtain a uniformly distributed spin configuration. It is well known that the skyrmions evolve from the stripe domain to the ferromagnetic state while increasing the magnetic field.[5,7,26–29] Usually the ground domain state *i.e.*

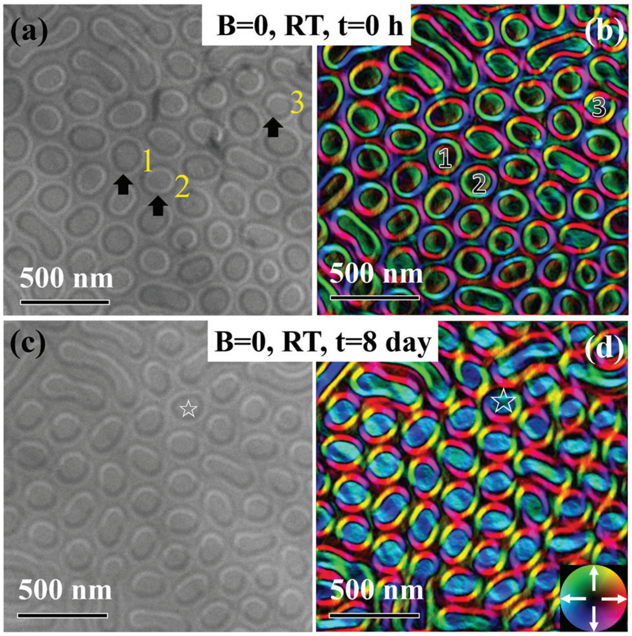

Fig. 5 The temporal evolution of the relaxation behaviour in the initial state (a) LTEM image and (b) corresponding spin textures obtained by TIE. (c) The uniform type II bubble distribution after relaxation and (d) the corresponding spin textures. The star indicates the only one type I bubble in the view region. The color wheel in the corner shows the magnetization directions.

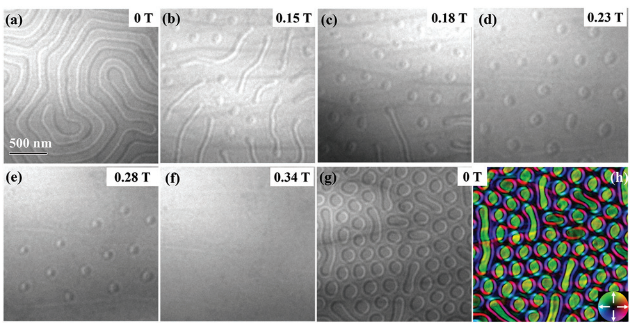

Fig. 6 Lorentz TEM images of magnetic bubble evolution with increasing magnetic field to (a) 0, (b) 0.15, (c) 0.18, (d) 0.23, (e) 0.28, and (f) 0.34 T at a fixed current density $J = 3.36 \times 10^7$ A m^{-2}. (g) The residual magnetic domain distribution and (h) corresponding spin texture by TIE analysis after switching off the magnetic field at the fixed current density, displaying uniform type II bubbles and dumbbells.

stripes or labyrinth domain instantly pops out from the homogeneous ferromagnetic state when decreasing the magnetic field. However, the intermediate skyrmion or bubble phase can be tuned out from the ferromagnetic state if an appropriate electric current interferes with the phase transition when decreasing the magnetic field.[33] The magnetic field dependence of bubble evolution at a fixed current of 120 mA (current density $J = 3.36 \times 10^7$ A m^{-2}) is shown in Fig. 6a–g. The unchanged labyrinth in Fig. 6a indicates that the current density is not strong enough to alter the labyrinthine domain structure. With the assistance of further magnetic field, the bubbles appear at a magnetic field of 0.15 T (Fig. 6b) and become dominant at 0.18 T (Fig. 6c). The labyrinth domains are completely replaced by bubbles at about 0.23 T (Fig. 6d). Some skyrmions begin to vanish (Fig. 6e) and the saturated ferromagnetic state without any domain feature is observed at a magnetic field of 0.34 T (Fig. 6f). Due to the electric current interference, the magnetic fields required to generate and annihilate bubbles become lowered and furthermore, high-density uniform type II bubbles and dumbbells (Fig. 6g and h) are obtained in the residual state after switching off the magnetic field.

The electromagnetic manipulation is closely related to the interaction between conduction electrons and the diversified spin configurations, where the angular momentum or orientation of magnetization can be adjusted to generate and propagate the skyrmion (bubble) lattice if the spin transfer torque is strong enough.[16,44–46] The realization of the hexagonal magnetic bubble lattice at zero field and the diversified spin configuration *via* different electromagnetic manipulation procedures in MnNiGaY helps us to explore the universal phenomenon and mechanism. The abundant experiments stimulate theoretical study on the nature of the interaction between electric current and spin configurations, thereby instructing to get any spin configuration *via* manipulation in turn.

4. Conclusions

In summary, the evolution of the magnetic spin configuration is studied in MnNiGaY by means of LTEM. The substitution of rare earth element Y enhances the quality factor *Q* to generate magnetic bubbles instead of biskyrmions. Real-space imaging of the magnetization textures reveals the emergence of magnetic bubbles with random spin configurations originating from the freedom of spin helicity. Via different electromagnetic manipulation, the density of bubbles is controllable and a zero-field hexagonal bubble lattice is achieved under optimized conditions. In addition, uniform type II bubbles are observed after temporal relaxation or by altering the magnetic field at a fixed current density. The generation of the high-density field-free bubble lattice and the diverse manipulation from the random spin configuration to uniform type II bubbles *via* electromagnetic interactions microscopically broaden the horizon of exploring novel mechanisms and applications in nonvolatile memory devices.

Author contributions

B. G. Shen and Y. Zhang conceived and designed the experiments. S. L. Zuo performed the experiments. L. C. Peng contributed to the LTEM experiments. X. Zhao synthesized the samples. M. He contributed to the electric current control setup. R. Li and H. Li contributed to magnetization measurements. J. F. Xiong, J. R. Sun and F. X. Hu contributed to the result analysis. S. L. Zuo, Y. Zhang and T. Y. Zhao analysed the data and wrote the manuscript. All authors discussed the results and commented on the manuscript.

Conflicts of interest

There are no conflicts to declare.

Acknowledgements

This work was supported by the National Basic Research Program of China (Grant No. 2014CB643702), the National Key Research and Development Program of China (Grant No. 2016YFB0700902 and 2016YFB0700903) and the National Natural Science Foundation of China (Grant No. 51590880 and 11374349). The Knowledge Innovation Project of the Chinese Academy of Sciences (Grant No. KJZD-EW-M05) and the Youth Innovation Promotion Association, CAS, 2015004.

Notes and references

† As $\lambda \equiv l_c/h = [\gamma_w/(2K_d)]/h = (\gamma_w/\mu_0 M_S^2)/h$, we determine the characteristic length l_c and the specific domain wall energy γ_w in terms of stripe domain period P, given by $\gamma_w = 2P^2\mu_0 M_S^2 f(M)/[\pi^3 h(1 + \mu^{*1/2})]$, based on Kooy and Enz model,[32] where $\mu^* = 1 + 1/Q$, and $f(M)$ is a function of the magnetization distribution and takes a numerical value[32] of 1.052 while the stripe period was measured in demagnetized state. With P = 250 nm, h = 80 nm, and Q = 0.99 obtained previously, we have γ_w of 3.28 mJ m^{-2} for MnNiGaY, then l_c = 21.9 nm and λ = 0.274. The value of γ_w is quite consistent with the value of 3.09 mJ m^{-2} obtained by the definition $\gamma_w = 4(AK_u)^{1/2}$, where the exchange stiffness constant A is estimated in terms of Curie temperature T_C, with the commonly adopted formular[30] $A = 2k_B T_C S^2/(a_L \cdot z)$, where k_B is the Boltzmann constant, equals to 1.38×10^{-23} J/K, T_C is the Curie temperature, 350 K for both MnNiGa and MnNiGaY, S is the elementary spin quantum number (1/2), a_L the structural lattice constant (~0.5 nm, the distance between two Mn atoms alone c-axis), and z is a factor between 0.1 and 0.6, which results in the exchange stiffness constant A in the range from 8.05×10^{-12} to 4.83×10^{-11} J m^{-1}, being a similar range as other ferromagnetic materials. The specific domain wall energy γ_w is obtained in the range from 3.09 to 7.57 mJ m^{-2}, thus, the characteristic length l_c has a range from 20.7 nm to 50.6 nm for MnNiGaY.

1 S. Parkin, M. Hayashi and L. Thomas, *Science*, 2008, **320**, 190–194.
2 F. Jonietz, S. Mühlbauer, C. Pfleiderer, A. Neubauer, W. Münzer, A. Bauer, T. Adams, R. Georgii, P. Böni, R. A. Duine, K. Everschor, M. Garst and A. Rosch, *Science*, 2010, **330**, 1648–1651.
3 L. Thomas, R. Moriya, C. Rettner and S. S. P. Parkin, *Science*, 2010, **330**, 1810–1813.
4 N. Nagaosa and Y. Tokura, *Nat. Nanotechnol.*, 2013, **8**, 899–911.
5 X. Z. Yu, M. Mostovoy, Y. Tokunaga, W. Zhang, K. Kimoto, Y. Matsui, Y. Kaneko, N. Nagaosa and Y. Tokura, *Proc. Natl. Acad. Sci. U. S. A.*, 2012, **109**, 8856–8860.
6 D. Morikawa, X. Z. Yu, Y. Kaneko, Y. Tokunaga, T. Nagai, K. Kimoto, T. Arima and Y. Tokura, *Appl. Phys. Lett.*, 2015, **107**, 212401.
7 X. Z. Yu, Y. Tokunaga, Y. Taguchi and Y. Tokura, *Adv. Mater.*, 2017, **29**, 1603958.
8 P. J. Grundy and S. R. Herd, *Phys. Status Solidi A*, 1973, **20**, 295–307.
9 S. Herd and P. Chaudhari, *Phys. Status Solidi A*, 1973, **18**, 603–611.
10 P. J. Grundy, D. C. Hothersall, G. A. Jones, B. K. Middleton and R. S. Tebble, *Phys. Status Solidi A*, 1972, **9**, 79–88.
11 A. P. Malozemoff and J. C. Slonczewski, *Magnetic domain walls in bubble materials*, Academic Press, New York, 1979.
12 A. H. Eschenfelder, *Magnetic bubble technology, Springer series in Solid-State Sciences*, 1980, vol. 14.
13 A. Hubert and R. Schäfer, *Magnetic domain: The analysis of magnetic microstructures*, Springer-Verlag, Berlin Heidelberg, 1998, p. 391.
14 S. A. Montoya, S. Couture, J. J. Chess, J. C. T. Lee, N. Kent, D. Henze, S. K. Sinha, M. Y. Im, S. D. Kevan, P. Fischer, B. J. McMorran, V. Lomakin, S. Roy and E. E. Fullerton, *Phys. Rev. B*, 2017, **95**, 024415.
15 W. Jiang, P. Upadhyaya, W. Zhang, G. Yu, M. B. Jungfleisch, F. Y. Fradin, J. E. Pearson, Y. Tserkovnyak, K. L. Wang, O. Heinonen, S. G. E. te Velthuis and A. Hoffmann, *Science*, 2015, **349**, 283–286.
16 H. Nakajima, A. Kotani, K. Harada, Y. Ishii and S. Mori, *Phys. Rev. B*, 2016, **94**, 224427.
17 T. Garel and S. Doniach, *Phys. Rev. B: Condens. Matter Mater. Phys.*, 1982, **26**, 325–329.
18 S. Mülbaure, B. Binz, F. Jonietz, C. Pfleiderer, A. Rosch, R. Georgii, A. Neubarer and P. Boni, *Science*, 2009, **323**, 915–919.
19 C. Pappas, E. Lelievre-Berna, P. Falus, P. M. Bentley, E. Moskvin, S. Grigoriev, P. Fouquet and B. Farago, *Phys. Rev. Lett.*, 2009, **102**, 197202.
20 A. Neubauer, C. Pfleiderer, B. Binz, A. Rosch, R. Ritz, P. G. Niklowitz and P. Boni, *Phys. Rev. Lett.*, 2009, **102**, 186602.
21 A. Tonomura, X. Z. Yu, K. Yanagisawa, T. Matsuda, Y. Onose, N. Kanazawa, H. S. Park and Y. Tokura, *Nano Lett.*, 2012, **12**, 1673–1677.
22 X. Z. Yu, N. Kanazawa, Y. Onose, K. Kimoto, W. Z. Zhang, S. Ishiwata, Y. Matsui and Y. Tokura, *Nat. Mater.*, 2011, **10**, 106–109.
23 H. Wilhelm, M. Baenitz, M. Schmidt, U. K. Rossler, A. A. Leonov and A. N. Bogdanov, *Phys. Rev. Lett.*, 2011, **107**, 127203.
24 X. Z. Yu, Y. Onose, N. Kanazawa, J. H. Park, J. H. Han, Y. Matsui, N. Nagaosa and Y. Tokura, *Nature*, 2010, **465**, 901–904.
25 Y. S. Lin, J. Grundy and E. A. Giess, *Appl. Phys. Lett.*, 1973, **23**, 485.
26 X. Z. Yu, Y. Tokunaga, Y. Kaneko, W. Z. Zhang, K. Kimoto, Y. Matsui, Y. Taguchi and Y. Tokura, *Nat. Commun.*, 2014, **5**, 3198.
27 W. H. Wang, Y. Zhang, G. Xu, L. Peng, B. Ding, Y. Wang, Z. Hou, X. Zhang, X. Li, E. Liu, S. Wang, J. Cai, F. Wang, J. Li, F. Hu, G. Wu, B. Shen and X. Zhang, *Adv. Mater.*, 2016, **28**, 6887–6893.

28 C. Phatak, O. Heinonen, M. D. Graef and A. Petford-Long, *Nano Lett.*, 2016, **16**, 4141.
29 Z. Hou, W. Ren, B. Ding, G. Xu, Y. Wang, B. Yang, Q. Zhang, Y. Zhang, E. Liu, F. Xu, W. Wang, G. Wu, X. Zhang, B. Shen and Z. Zhang, *Adv. Mater.*, 2017, **29**, 1701144.
30 W. Jiang, G. Chen, K. Liu, J. Zang, S. G. te Velthuis and A. Hoffmann, *Phys. Rep.*, 2017, **704**, 4–19.
31 M. Finazzi, M. Savoini, A. R. Khorsand, A. Tsukamoto, A. Itoh, L. Duò, A. Kirilyuk, Th. Rasing and M. Ezawa, *Phys. Rev. Lett.*, 2013, **110**, 177205.
32 K. Y. Guslienko, *IEEE Magn. Lett.*, 2015, **6**, 1–4.
33 L. C. Peng, Y. Zhang, M. He, B. Ding, W. H. Wang, H. F. Tian, J. Q. Li, S. G. Wang, J. W. Cai, G. H. Wu, J. P. Liu, M. J. Kramer and B. G. Shen, *NPJ Quant. Mater.*, 2017, **2**, 30.
34 T. Schulz, R. Ritz, A. Bauer, M. Halder, M. Wagner, C. Franz, C. Pfleiderer, K. Everschor, M. Garst and A. Rosch, *Nat. Phys.*, 2012, **8**, 301.
35 N. Romming, C. Hanneken, M. Menzel, J. E. Bickel, B. Wolter, K. von Bergmann, A. Kubetzka and R. Wiesendanger, *Science*, 2013, **341**, 636–639.
36 J. Sampaio, V. Cros, S. Rohart, A. Thiaville and A. Fert, *Nat. Nanotechnol.*, 2013, **8**, 839–844.
37 M. Mochizuki, *Phys. Rev. Lett.*, 2012, **108**, 017601.
38 L. Y. Kong and J. D. Zang, *Phys. Rev. Lett.*, 2013, **111**, 067203.
39 M. Mochizuki, X. Z. Yu, S. Seki, N. Kanazawa, W. Koshibae, J. Zang, M. Mostovoy, Y. Tokura and N. Nagaosa, *Nat. Mater.*, 2014, **13**, 241–246.
40 L. Peng, Y. Zhang, W. Wang, M. He, L. Li, B. Ding, J. Li, Y. Sun, X.-G. Zhang, J. Cai, S. Wang, G. Wu and B. Shen, *Nano Lett.*, 2017, **17**, 7075–7079.
41 G. Asti and S. Rinaldi, *Phys. Rev. Lett.*, 1972, **28**, 1584–1586.
42 G. Asti and S. Rinaldi, *J. Appl. Phys.*, 1974, **45**, 3600–3610.
43 G. Asti and F. Bolzoni, *J. Appl. Phys.*, 1985, **58**, 1924–1934.
44 H. Callen and R. M. Josephs, *J. Appl. Phys.*, 1971, **42**, 1977–1982.
45 J. C. Slonczewski, *J. Magn. Magn. Mater.*, 1996, **159**, L1–L7.
46 L. Berger, *J. Appl. Phys.*, 1984, **55**, 1954–1956.

